Experimental Research on the Performance of a Novel Geo- filament Anchor for an Earthen Architectural Site

Wang Yulan (ylwhbp@xauat.edu.cn)
Xi'an University of Architecture & Technology
Guo Jian
Xi'an University of Architecture & Technology
Zhang weixi
Xi'an University of Architecture & Technology
Lei Fan
Shaanxi Provincial Institute of Cultural Heritage

Research Article

Keywords: Earthen architecture ruins, Small sliding mass, Geo-filament anchor (GFA), In-situ test, Design concept

Posted Date: March 7th, 2022

DOI: https://doi.org/10.21203/rs.3.rs-951337/v2

Experimental Research on the Performance of a Novel Geo-filament Anchor for an Earthen Architectural Site

Wang Yulan[a,b*], *E-mail address: ylwhbp@xauat.edu.cn*; Guo Jian[a,b], *E-mail address:*346535527@qq.com;

Zhang weixi[c], E-mail address:81941216@qq.com; Lei Fan[d] , E-mail address:576808036@qq.com

[a] *State Key Laboratory of Green Building in Western China，Xian University of Architecture & Technology，Xi'an 710055, China,*

[b] *Architecture College, Xi'an University of Architecture & Technology, Xi'an 710055, China*

[c]*Science College，Xi'an University of Architecture and Technology，Xi'an 710055，China*

[d]*Shaanxi Provincial Institute of Cultural Heritage, Xi'an 710075,china*

ABSTRACT:

An efficient anchoring method, explicitly developed for small sliders, has hitherto been missing in the practice of earthen architecture conservation. Furthermore, anchorage performance studies conducted so far, have failed to fully take into account the soil characteristics of certain targets. To address these concerns, the conservation project conceived for the Gaochang Ruins, Turpan, in China, was selected as the experiment ground to design a novel Geotechnical Filament Anchor (GFA) for reinforcing small sliders in the earthen historical ramparts. In-situ experiments were conducted for evaluating six parameters—anchorage length (L), GF thickness (H), bore diameter (D), slurry strength (S), GFA surface status (R), and inclination angle (A). These parameters were varied in order to determine the effect they produce on anchorage performance, as demonstrated by the indicators, including tensile strength, destruction mode, load displacement (P-S) relation, and strain (ζ-L) distribution characteristics of the novel GFA. Data acquired from the experiments, in combination with the conservation specifics of earthen architectural sites, anchorage performance, and safety reserve, were further employed to introduce a calculation formula for computing the designed force value (N) through L. A simplified model depicting the shear stress distribution of the anchorage system under N was devised by extracting the strain distribution data with respect to the GF-slurry interface. Taking into account the soil properties of the above-mentioned site, the shear stress diffusion coefficient (α) was conceptualized, the formula for the shear strength of the grouting material was devised, and the tolerable ranges of L, D, H, R, and S were determined. A new design idea is proposed for the application of anchorage technology in earthen ruins in combination with the characteristics of cultural relics protection, which certainly promotes the formation of its design concept and calculation method.

KEYWORDS: *Earthen architecture ruins; Small sliding mass; Geo-filament anchor (GFA); In-situ test; Design concept*

1. Introduction:

Earthen architectural sites remain one of the most treasured cultural legacies for the whole of humankind. Keeping in mind the diversities present in the construction materials, vulnerability, structural complexity, and varied classifications of earthen architectural sites, cultural relics protection entities, constantly face the challenge of safeguarding and maintaining these historical remnants[1].

At present, measures combining support and anchorage are mainly taken for structure stability of earthen architecture ruins for reinforcement. The anchorage technology is widely applied in the geotechnical engineering field, and a large number of laboratory and field test results have been obtained through the research on anchorage performance, theory for mechanics of interface, anchorage parameter and other aspects of reinforcement, steel strand, GFRP and AFRP and other rods[2-8]. However, the reinforcement on the structure of earthen architecture ruins is special, and the reinforcement technology and material adopted in other fields cannot be totally copied and applied.

Therefore, a new anchor rod for the reinforcement on the structure of earthen architecture ruins has been developed and applied[9-11]. The anchorage objects are mostly the medium and large sliding masses in earthen architecture ruins, and the rod is mainly made of phyllostachys pubescens, wood, reinforcement and others[12-15]. Relevant researches mostly focus on the influence of anchor rod length and grouting material on anchorage force and the research on stress distribution characteristics of rod-slurry interface[16-24]. However, the requirements of soil characteristics of reinforced ruins on anchorage performance are not fully considered, the special anchorage measures are not taken for small sliding masses, there is no corresponding design theory and calculation method for anchorage technology of earthen ruins, and the design basis is mostly based on experience and test data.

In this paper, a new GFA is designed by taking the reinforcement of small sliding mass as the research background through the summary of the application and R&D experience of anchorage technology in the protection of Gaochang Ruins to research its tensile strength, destruction mode and the distribution characteristics of load displacement (P-S) relation and strain (ζ-L) through the control of changes of 6 parameters of anchorage length (L), GF thickness (H), bore diameter (D), slurry strength (S), GFA surface state (R) and inclination angle (A), conduct corresponding analysis for the test data and phenomena, try to summarize the design concept and calculation method of GFA, and simultaneously discuss and rethink the application and development of anchorage technology of earthen ruins.

2. Research background:

Gaochang Ruins, one of the important ruins in the Silk Road, was built in the first century BC (middle years of the Western Han Dynasty) and abandoned in the late 13th century due to war, its usage period is more than one thousand three hundred years and it has been more than two thousand years since it was built.

Most existing rampart ruins are reconstructed and built on the basis of Gaochang City in Tang Dynasty. The whole city is an irregular square (as shown in Figure 1), with a floor area of about 198 ha. It is composed of three parts: outer city, inner city and imperial city. The rampats is 6-11m high and about 10 m wide (bottom), which is rammed and built with raw soil, with the thickness of tamping layer of 8 - 10 cm. Due to the natural and man-made destruction over one hundred years, the rampart ruins are damaged to varying degrees (as shown in Figure 2)

In this paper, on the research background of reinforcement protection for rampart ruins of Gaochang Ruins, five large-scale protection projects have been performed for the protection of earthen ruins of Gaochang Ruins since 2005, and grouting, adobe support, anchor rod reinforcement and other technical measures are mainly taken for the reinforcement on the structure of rampart ruins.

The reinforced anchor rod is mostly made of bamboo or wood. Such anchor rods can provide greater anchorage force, and effectively control the displacement. They can give full play to their advantages when reinforcing the potential large-scale sliding masses (as shown in Figure 3), with certain requirements on opening depth and diameter. The problem of excessive intervention will occur when they are used to reinforce small sliding masses (as shown in Figure 4). In view of the above problems, a new GFA is designed for the reinforcement of small sliding masses of rampart ruins of Gaochang Ruins.

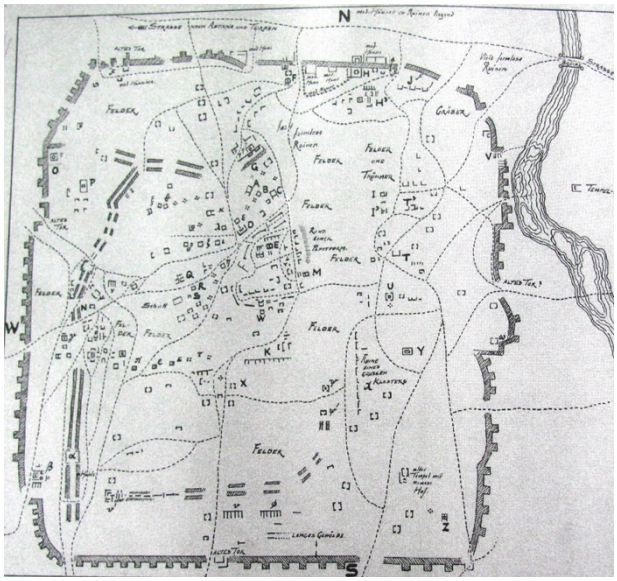

（a）Marc Aurel Stein 's hand drawing(1907).

（b）Vertical photograph.

Fig.1 The plane layout of the Gaochang Ruins.

Fig.2 The partial status of outer rampart ruins of Gaochang.

Fig.3 The potential large-scale sliding masses.

Fig.4 The potential small sliding masses.

3. Experiment scheme:

Geo-filament is a high-fiber synthetic material, which can form the stiffed belt after extrusion molding, as shown in Figure 5. The tensile strength of geo-filament is very high, and all its physical and mechanical indexes are shown in Table 1.

Fig.5 Geo-filament.

Table 1 GF material performance

Ultimate tension *kN*	*Tensile strength* *MPa*	*Elongation* *%*	*Friction coefficient* *f*
20.5	*273*	*1.4*	*0.6*

3.1 Experiment design and specimen preparation:

To research the influence of changes of anchor rod length (L), thickness (H), bore diameter (D), grouting material (S), ribbing spacing (R) and arrangement angle (A) (the angle between the opening axis and the horizontal direction) on the anchorage performance, it is designed with 6 independent test batches, including 19 groups of tests in total, of which 3 test pieces are processed in each group of test. The single-factor test method was adopted, where the effect of a single factor on the anchorage force at a given time is evaluated under similar environmental conditions, keeping the other five factors as constant.

The six independent test batches are respectively: anchor length L *(5 groups); thickness* H *(3 groups); bore diameter* D *(3 groups); grouting strength* S *(3 groups); ribbing spacing* R *(3 groups); arrangement angle* A *(3 groups). The test grouping design parameters are shown in Table 2.*

Cut the geo-filament according to the test needs, with 400 mm free section reserved for the anchorage of drawing instruments. Evenly wind ribbing outside of anchor rod with hemp rope, with the spacing determined by the test scheme, wind the ends for three layers, and then evenly paint with the epoxy resin. It is necessary to ensure that the hemp rope is completely soaked by the epoxy resin during painting, so that it can be closely connected with geo-filament.

To test the geo-filament-slurry interface stress distribution, divide the filament anchor rod into four equidistant sections, arrange the strain gauge at ends and demarcation points, and set the compensating plate in the middle of the anchor rod. The schematic diagram of anchor production is shown in Figure 6. The diagram of the cross section of the anchor is shown in Figure 7. Seal and protect the strain gauge with epoxy resin and waterproof tape, and number it after welding the lead and shielded conductor. The field production of test piece is shown in Figure 8.

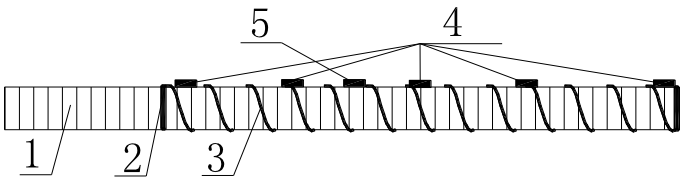

Fig.6 The experiment anchor rod diagram.
1. geo-filament；2. three times of hemp rope；3. hemp rope；4. strain foils；5. compensator

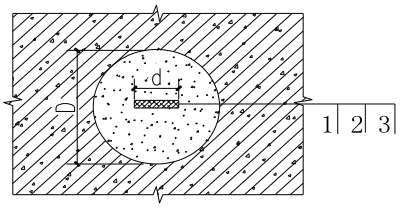

Fig.7 Diagram of the cross section of the anchor.
1. geo-filament; 2. grout; 3.site soil

a Winding of Hemp Rope *b Painting of Epoxy Resin* *c Pasting of Strain Gauge* *d Molding of Anchor Rod*

Fig.8 The manufacture of experiment anchor rod.

Table 2 Specimen grouping design parameter table

Parameter / Factor	Anchor length (mm)	thickness (piece)	Bore diameter (mm)	Slurry number	Ribbed spacing（mm）	Angel of inclination(°)	Number of test pieces
L Series（Anchor length）	800（L8）	Single	45	S2	30	0°	3
	1200（L12）						3
	1500（L15）						3
	2000（L20）						3
	3000（L30）						3
H Series（One-sided thickness）	1200	Single（H1）	45	S2	30	0°	3
		Double root（H2）					3
D Series（Aperture）	1200	Single	45（D45）	S2	30	0°	3
			75（D75）				3
			80（D80）				3
S Series（Slurry strength）	1200	Single	45	S1	30	0°	3
				S2			3
				S3			3
R Series（Ribbed spacing）	1200	Single	45	S2	0（R0）	0°	3
					30（R30）		3
					100（R100）		3
A Series（slope）	1200	Single	45	S2	30	0°（A0）	3
						10°（A10）	3
						15°（A15）	3

3.2 Material characteristics of the experiment:

(1) Mechanical properties of the rammed earth:

The rampart relics of Gaochang are mainly built with rammed earth. To reduce the test deviation, drill core samples in the in-situ test area, and measure the parameters of rammed earth materials, as shown in Table 3.

Table 3 Physical and mechanical parameters of rammed earth

Test lock	*Moisture content ω /%*	*Density ρ /g•cm^{-3}*	*Angle of internal friction φ /(°)*	*Cohesion strength c /kN*	*Test block compressive strength (MPa)*	*Compression Elastic Modulus E/MPa*
1	*3.2*	*1.89*	*25.5*	*28.5*	*1.61*	*180.32*
2	*2.8*	*1.76*	*23.6*	*27.6*	*1.55*	*179.40*
3	*2.5*	*1.81*	*24.4*	*28.2*	*1.73*	*188.80*
Mean	*2.8*	*1.82*	*24.5*	*28.1*	*1.63*	*182.84*

(2) Mechanical properties of the grouting body:

Three kinds of slurry are prepared according to the actual engineering experience (S1, S2, S3), and the slurry proportion is calculated according to the weight proportion.

Proportion of S1 earth: cement: fly ash = 90:5:5. 5% ludox emulsion is mixed.

Proportion of S2 earth: cement: fly ash = 85:5:10. 5% sweller is used.

Proportion of S3 earth: cement: fly ash = 80:10:10. 5% sweller emulsion is mixed.

The water cement ratio of three kinds of slurry is 30% (weight ratio). Make slurry test blocks with 7.07 × 7.07 mm mortar test mold, and measure its compressive mechanical property 30 days after curing, as shown in Table 4.

Table4 Mechanical properties of grout

Test block	*Number*	*Compressive Strength (MPa)*		*Compression Elastic Modulus (MPa)*	
		Experimental value	*average*	*Experimental value*	*average*
SI grout	*1*	*1.94*	*1.93*	*65.65*	*64.89*
	2	*1.86*		*63.26*	
	3	*1.98*		*65.78*	
S2 grout	*1*	*2.81*	*2.81*	*68.75*	*68.60*
	2	*2.72*		*67.38*	
	3	*2.91*		*69.68*	
S3 grout	*1*	*5.64*	*5.41*	*188.5*	*184.06*
	2	*5.32*		*182.3*	
	3	*5.27*		*181.4*	

4. In-situ test:

4.1 Test piece installation:

To avoid the interaction among anchor rods, the drilling spacing in vertical and horizontal directions shall be more than 1 m. Clear the bore diameter with brush and hair dryer. The grouting pressure of grouter is 0.5 MPa to ensure the dense pouring of slurry and the grouting material (modified loess slurry) with a depth of 100 mm shall be used at pore ends for dense pouring.

4.2 Test method:

The measurement range of anchor rod tension meter is 0-100 kN, the pull stroke is 150 mm, and the model is ZY-10. The strain acquisition instrument shall be TDS-303 data acquisition instrument produced by Japan, with the measurement range from －20,000 to 20,000. The KFG series general foil strain gauge is used, and the dimension of sensitive grid is 3 × 10 mm (with the resistance value of 120.8±0.1 and the sensitivity of 2.14 ± 1%). To cooperate with the anchor rod tension meter, make counterforce frame with thick steel plate. The middle of the counterforce frame and the ruins are padded with wood block, and the displacement sensor is installed on the steel counterforce frame. The schematic diagram of test device is shown in Figure 9.

The test is performed in the primary soil of non-cultural relics near the eastern section of northern rampats of Gaochang Old City in Turpan, Xinjiang in May. Considering location and climate factors, the in-situ pull-out test is performed after the anchor rod is implanted and the slurry is completely consolidated (about 40 days).

To eliminate the stress clearance among devices, 200N pull shall be pre-applied before data acquisition. The method of electric servo hydraulic pressure is adopted for loading, and the loading rate is 50N/s until the anchorage system is damaged.

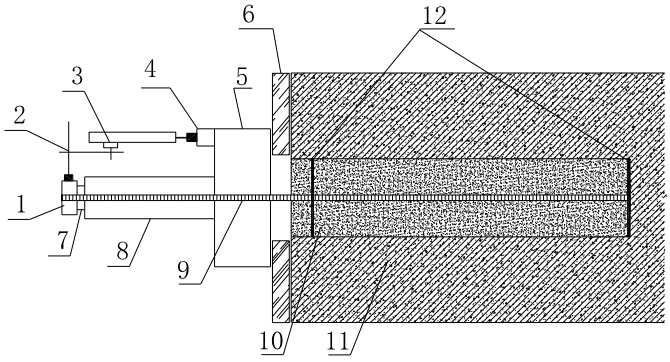

Fig9 The experimental device diagram.
1. anchorage, 2. magnetic stand, 3. displacement sensor, 4. the support displacement sensor, 5. reaction frame, 6. wood footplate, 7. load sensor, 8. hollow jack, 9. Geo-filament bolt, 10.grouting material, 11. site soil；12. locating ring.

5. Analysis of the test results:

5.1 Analysis of the anchorage performance:

According to the test phenomenon, record and collect the test data, and obtain all failure stages and ultimate anchorage forces during pull-out process of GFA of each test group, as shown in Tables 5 - 10 (data with "" in the table is bad value).*

Table 5 The test results by different anchor rod length.

Number	Destruction mode（kN）	Fracture load（kN）	Average（kN）
L8-1	GF deformation（2.3）→slurry cracking（6.8）→GF pull out（7.8）	7.8	
L8-2	GF deformation（1.6）→slurry cracking（5.2）→GF pull out（5.4）	5.4*	7.95
L8-3	GF deformation（2.2）→slurry cracking（7.3）→GF pull out（8.1）	8.1	
L12-1	GF deformation（2.3）→slurry cracking（7.6）→GF pull out（11.5）	11.5	
L12-2	GF deformation（2.4）→slurry cracking（7.8）→GF pull out（9.8）	9.8	10.63
L12-3	GF deformation（2.0）→slurry cracking（8.1）→GF pull out（10.6）	10.6	
L15-1	GF deformation（2.3）→slurry cracking（6.5）→slurry crushing（11.2）→GF pull out（15.5）	15.5	
L15-2	GF deformation（2.5）→slurry cracking（7.1）→slurry crushing（13.6）→GF pull out（17.1）	17.1	16.47
L15-3	GF deformation（2.3）→slurry cracking（7.5）→slurry crushing（12.8）→GF pull out（16.8）	16.8	
L20-1	GF deformation（2.3）→slurry cracking（7.5）→slurry crushing（12.3）→GF pull out（18.7）	18.7	
L20-2	GF deformation（2.8）→slurry cracking（8.2）→slurry crushing（15.1）→GF pull out（15.6）	15.6*	18.55
L20-3	GF deformation（2.3）→slurry cracking（7.3）→slurry crushing（11.8）→GF pull out（18.4）	18.4	
L30-1	GF deformation（2.6）→slurry cracking（7.8）→slurry crushing（11.5）→GF fracture（19.8）	19.8	
L30-2	GF deformation（2.4）→slurry cracking（7.5）→slurry crushing（13.2）→GF fracture（19.6）	19.6	19.83
L30-3	GF deformation（2.2）→slurry cracking（8.2）→slurry crushing（12.8）→GF fracture（20.1）	20.1	

Table 6 Test results of different anchor rod thickness.

Number	Destruction mode（kN）	Fracture load（kN）	Average（kN）
H1-1	GF deformation（2.5）→slurry cracking（8.0）→GF pull out（10.6）	10.6	
H1-2	GF deformation（2.5）→slurry cracking（8.2）→GF pull out（11.7）	11.7	11.16
H1-3	GF deformation（2.2）→slurry cracking（7.5）→GF pull out（11.2）	11.2	
H2-1	GF deformation（3.2）→slurry cracking（7.5）→slurry crushing（12.3）→GF pull out（14.2）	14.2	
H2-2	GF deformation（3.5）→slurry cracking（7.1）→slurry crushing（12.6）→GF pull out（13.6）	13.6	13.53
H2-3	GF deformation（3.5）→slurry cracking（7.9）→slurry crushing（11.8）→GF pull out（12.8）	12.8	

Table 7 The test results by different bore diameter.

Number	Destruction mode（kN）	Fracture load（kN）	Average（kN）
D45-1	GF deformation（2.3）→slurry cracking（7.4）→GF pull out（11.5）	11.5	
D45-2	GF deformation（2.1）→slurry cracking（7.8）→GF pull out（10.1）	10.1	10.77
D45-3	GF deformation（2.2）→slurry cracking（7.5）→GF pull out（10.7）	10.7	
D75-1	GF deformation（2.4）→slurry cracking（6.3）→GF pull out（8.1）	8.1*	
D75-2	GF deformation（2.5）→slurry cracking（6.5）→GF pull out（10.7）	10.7	10.5
D75-2	GF deformation（2.2）→slurry cracking（6.6）→GF pull out（10.3）	10.3	
D80-1	GF deformation（2.3）→GF pull out（7.6）	7.6	
D80-2	GF deformation（2.2）→GF pull out（8.2）	8.2	7.63
D80-3	GF deformation（2.7）→GF pull out（7.4）	7.4	

Table 8 The test results by different slurry strength.

Number	Destruction mode（kN）	Fracture load（kN）	Average（kN）
S1-1	GF deformation（2.3）→slurry cracking（4.5）→GF pull out（7.3）	7.3	7.73
S1-2	GF deformation（2.5）→slurry cracking（3.7）→GF pull out（7.9）	7.9	

S1-3	GF deformation（2.1）→slurry cracking（4.3）→GF pull out（7.7）	7.7	
S2-1	GF deformation（2.1）→slurry cracking（7.5）→GF pull out（11.4）	11.4	
S2-2	GF deformation（2.3）→slurry cracking（8.2）→GF pull out（12.1）	12.1	11.43
S2-3	GF deformation（1.7）→slurry cracking（7.1）→GF pull out t（10.8）	10.8	
S3-1	GF deformation（2.1）→soil-part loosening（14.7）→slurry pull out（17.9）	17.9	
S3-2	GF deformation（1.8）→soil-part loosening（14.1）→slurry pull out（17.5）	17.5	17.53
S3-3	GF deformation（1.9）→soil-part loosening（13.3）→slurry pull out（17.2）	17.2	

Table 9 The test results by different surface state.

Number	Destruction mode（kN）	Fracture load（kN）	Average（kN）
R0-1	GF deformation（2.1）→GF pull out（4.7）	4.7	
R0-2	GF deformation（2.3）→GF pull out（4.5）	4.5	4.33
R0-3	GF deformation（2.0）→GF pull out（3.8）	3.8	
R30-1	GF deformation（2.0）→slurry cracking（7.5）→GF pull out（11.4）	11.4	
R30-2	GF deformation（2.4）→slurry cracking（7.7）→GF pull out（10.6）	10.6	11.06
R30-3	GF deformation（2.1）→slurry cracking（7.2）→GF pull out（11.2）	11.2	
R100-1	GF deformation（2.2）→GF pull out（7.3）	7.3	
R100-2	GF deformation（2.0）→GF pull out（7.5）	7.5	7.53
R100-3	GF deformation（2.4）→GF pull out（7.8）	7.8	

Table 10 The test results by different deployment angle of anchor rod.

Number	Destruction mode（kN）	Fracture load（kN）	Average（kN）
A0-1	GF deformation（2.0）→slurry cracking（7.2）→GF pull out（10.3）	10.3	
A0-2	GF deformation（2.2）→slurry cracking（8.1）→GF pull out（11.2）	11.2	10.77
A0-3	GF deformation（2.3）→slurry cracking（7.6）→GF pull out（10.8）	10.8	
A10-1	GF deformation（1.8）→slurry cracking（6.3）→GF pull out（9.4）	9.4	
A10-2	GF deformation（2.0）→slurry cracking（7.5）→GF pull out（10.2）	10.2	8.97
A10-3	GF deformation（2.1）→slurry cracking（6.6）→GF pull out（7.3）	7.3	
A15-1	GF deformation（1.9）→slurry cracking（4.7）→GF pull out（7.1）	7.1	
A15-2	GF deformation（2.3）→slurry cracking（5.1）→GF pull out（6.7）	6.7	6.37
A15-3	GF deformation（2.0）→slurry cracking（4.6）→GF pull out（5.3）	5.3	

Through the summary of test phenomena, it is found that the destruction mode is't single but multiple from the beginning of pull-out to the final destruction. The destruction mode when the anchorage system generates large displacement is regarded as the final failure type of the anchorage system. Four main failure types can be obtained as follows: geo-filament pullout (Figure 10a); slurry damage (Figure 10b); geo-filament fracture (Figure 10c); soil-part loosening and grouting material pullout (Figure 10d).

（a）GF pull out　（b）grouting damage　(c) GF fracture　(d) soil-part loosening and grouting material pullout

Fig10 The main destruction mode.

By summarizing of the destruction phenomena and the properties of each destruction stage, the following conclusions can be drawn:

a. *The destruction mode of the anchorage system is mainly the damage between the filament and the grouting material interface. Only with the robust strength level of the slurry can the slurry-soil interface damage be triggered, there exists complete exertion of the anchorage system force at this moment. Hence, the slurry-soil interface damage appears to be an ideal destruction mode, However,*

it can lead to the destruction of the site itself, hence, such a destruction mode appears non-conducive for heritage protection.

b. *When the length of anchorage reaches about 3,000 mm, the ultimate anchorage force is close to the breaking force of geo-filament, and the destruction mode of geo-filament fracture occurs.*

c. *The anchorage system of GFA, anchorage length (L), grouting material strength (S) and surface state (R) are more sensitive to the improvement of anchorage performance; the improvement of anchorage performance is not sensitive to anchor thickness (H), bore diameter (D) and anchorage angle (A).*

5.2 Load - displacement (P-S) relationship:

*Sort out the measured data of all tests, reject the bad value, and average the available data. The load displacement curves (*P-S*) of* L, H, D, R, S *and* A *are obtained respectively, as shown in Figures 11 - 16. According to the characteristics of each destruction stage of the anchorage system, the load displacement curves are distinguished by different colors.*

a. *The green area of the load-displacement curve represents the geo-filament deformation stage. The maximum load at this stage is expressed as* N_i.

b. *The yellow area of the load-displacement curve represents the stage where the grouting material crack or the pullout appears. The maximum load at this stage is expressed as* N_j.

c. *The red area of the load-displacement curves represents the stage of geo-filament pullout or fracture. The maximum load at this stage is expressed as* N_k.

(1) Influence of anchorage length L on the load-displacement curve.

The L-P-S *curve is shown in Figure 11. With the increase of anchor length, the anchorage force is significantly improved, and the anchor displacement is effectively controlled under the same pulling force.*

The anchorage force increases with the increase of anchor length. If the anchor length is in the range of 800 mm - 1,500 mm, the growth rate of ultimate anchorage force increases step by step, if the anchor length is in the range of 1,500 mm - 3,000 mm, the growth rate of ultimate anchorage force decreases; if the anchor length is about 3,000 mm, the ultimate anchorage force is close to the breaking force of geo-filament.

(2) Influence of geo-filament thickness H on the load-displacement curve.

The H-P-S *curve is shown in Figure 12. The thickness of* H2 *is twice that of* H1*, and the ultimate anchorage force increases by 17.5%, but the increase of geo-filament thickness cannot effectively control the displacement. The improvement of anchorage performance is not obvious by changing* H.

Because the geometry of the geo-filament is flaky, the strength of the soil in the anchorage system is higher than that of the grouting material, and the increase of the thickness (H) has a certain weakening effect on the integrity of the slurry. Through the test phenomenon, it can be concluded that the increasing of geo-filament thickness has little effect on the improvement of the anchorage performance; on the contrary, the breaking of the slurry is accelerated.

(3) Influence of bore diameter D on the load displacement curve

The D-P-S *curve is shown in Figure 13. The increase of bore diameter (*D*) leads to the increase of slurry proportion and radial dry shrinkage of the anchorage system, resulting in the decrease of radial pressure of the grouting material, thus weakening the bond strength between the geo-filament and the slurry interface, resulting in the increase of bore diameter, the early failure of the anchorage system for quitting working and the decrease of anchorage force, and the increase of bore diameter in practical engineering will cause great destruction to the cultural relics.*

(4) Influence of grouting strength S on the load displacement curve.

The S-P-S *curve is shown in Figure 14. The pull-out bearing capacity of anchor increases with the increase of strength grade of grouting material. It is mainly because that the strength of grouting material increase, the bond strength between slurry-rod interface be improved. Under the same tensile force, the displacement of* S1 *and* S2 *anchorage systems is about twice that of* S3 *anchorage system, indicating that increasing the strength of grouting material can effectively control the displacement.*

(5) Influence of anchor rod surface state R on the load displacement curve.

The R-P-S *curve is shown in Figure 15. The maximum anchorage force of without rib anchor rod* R0 *is 4.33 kN, and the maximum anchorage forces with rib of anchor* R100 *and* R30 *are 7.53 kN and 11.06 kN respectively. The ultimate anchorage force is 73.90% and 155.42% higher than that of without rib anchor rod respectively. When the tensile force reaches 3 kN, the displacement of ribbed anchorage system is significantly less than that of without rib anchorage system. It shows that changing the surface state of geo-filament can not only effectively improve the ultimate anchorage force, but also effectively control the displacement.*

(6) Influence of anchorage arrangement angle A on the load displacement curve.

The A-P-S *curve is shown in Figure 16. When the arrangement angle is 0º, the ultimate pull-out force of the anchor is the largest; with the increase of the arrangement angle, the ultimate pull-out force of the anchor decreases, because the applied load is horizontal. The larger the arrangement angle is, the greater the vertical component force is, and the anchorage volume cannot give full play to its anchorage performance. However, considering the requirements of construction process, it is suggested that the arrangement angle of anchor should be 10º.*

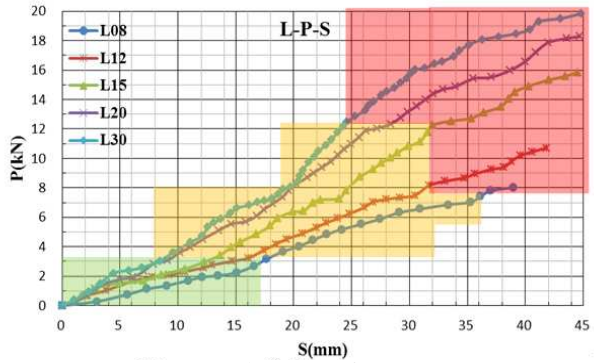

Fig11 The curve of L-P-S.

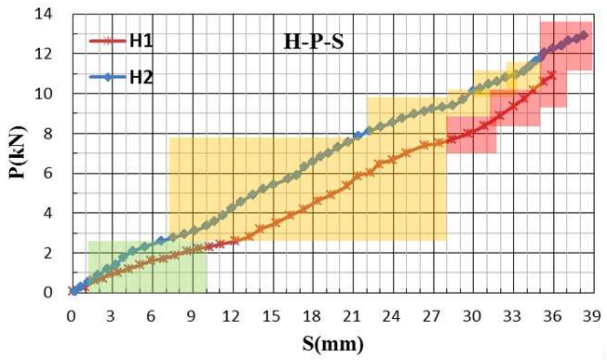

Fig 12 The curve of H-P-S.

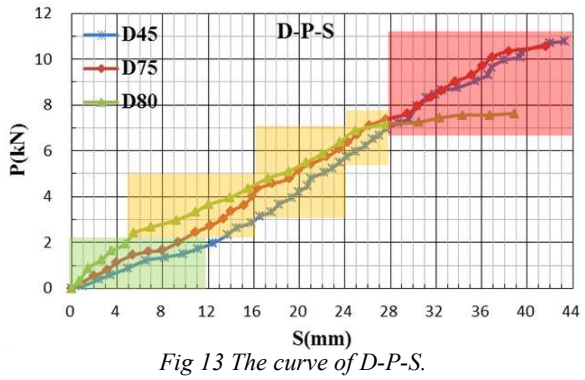

Fig 13 The curve of D-P-S.

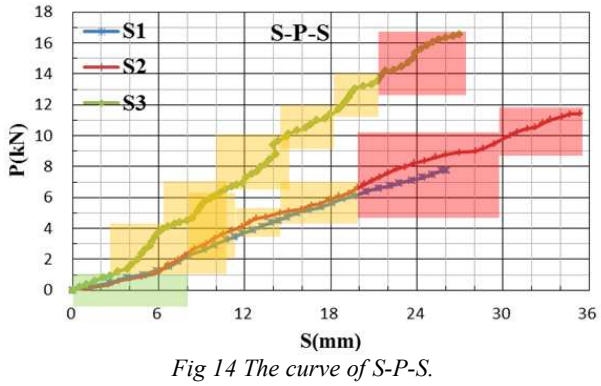

Fig 14 The curve of S-P-S.

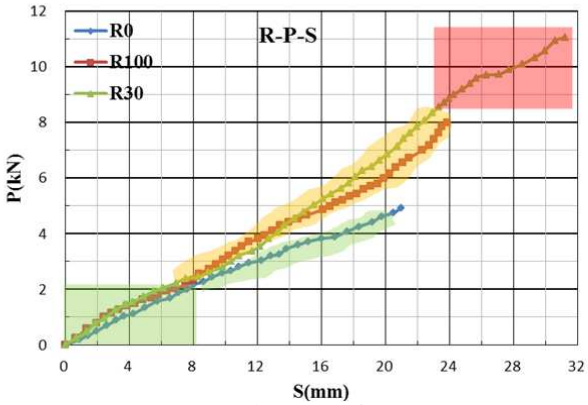

Fig 15 The curve of R-P-S.

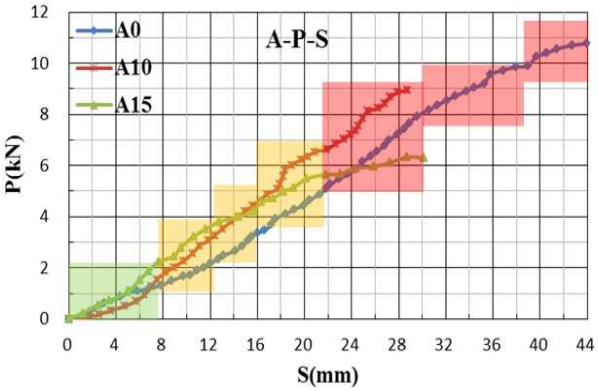

Fig 16 The curve of A-P-S.

5.3 Strain distribution ($\xi - L$) characteristics of GF - grouting interface:

According to the destruction results in the test, the failure of geo-filament anchorage system is caused by the pull-out of the anchor due to the bond-slip between the geo-filament and the slurry interface. The bond-slip section is in the red area of the P-S *curve (Figures 11-16). The failure of this section is similar to the brittle failure. There is no obvious deformation of the anchorage system, and the anchor is suddenly pulled out.*

In view of the particularity of the protection project of earthen architecture ruins, the performance of geo-filament anchorage system can be brought into full play. According to the test phenomenon and test results, the anchorage force design value N *of geo-filament anchor for strengthening earthen architecture ruins is determined. The selection of* N *value not only needs to meet the safety stock requirements of cultural relics protection projects, but also needs to give play to the anchorage performance of the anchorage system.*

According to the load displacement curve, the value N *is discussed by combination of the test phenomenon and the characteristics of strain distribution ($\xi - L$) at geo-filament-grouting interface. Considering the safety stock of anchorage system, the calculation formula of* N *value is shown in Formulas (1) or (2):*

$$N_1 = N_i + (N_j - N_i) \times 50\% \qquad (1)$$

$$Or \qquad N_2 = N_j + (N_k - N_j) \times 30\% \qquad (2)$$

Where N_i represents the extreme value of geo-filament deformation section, and the anchorage system is in the elastic stage; N_j represents the extreme value when the grouting is cracked or pulled out, and the anchorage system is in the plastic stage; N_k is the extreme value of geo-filament pull-out section, and the anchorage system is in the bond-slip stage.

The specific values of N_i, N_j and N_k are shown in Tables 5-10; N_1 and N_2 values of different test batches (L, H, D, S, R and A) can be obtained from Formulas (1) and (2). The anchor enters the bond stage from plastic that is an important manifestation of the anchorage system being about to fail; therefore, the extreme value N_j when the grouting is cracked or pulled out is compared with N_1 and N_2. The sorting out of value is shown in Table 11.

According to the data in Table 11, in most cases, $N_1 < N_j$. When N_1 is taken as the anchorage force design value, the performance of anchor is not fully brought into play. Therefore, no further consideration is made in data analysis, and the data not further processed in Table 11 is marked with "". The strain distribution curves of geo-filament-grouting interface of all test batches (L, H, D, R, S and A) corresponding to other values in Table 11 are extracted respectively, as shown in Figures 17 - 22.*

Table 11The N values in different experimental lots.

Classification			*N values (kN)*		
L	L8	L12	L15	L20	L30
N_1（*kN*）	4.65	5.03*	7.45*	7.18*	7.45*
N_2（*kN*）	7.32	8.67	13.71	14.00	14.69
N_j（*kN*）	7.45*	7.83	12.53	12.05	12.50
H	H1	H2	—	—	—
N_1（*kN*）	5.15*	7.82*	—	—	—
N_2（*kN*）	8.88	12.26	—	—	—
N_j（*kN*）	7.90	12.23			
D	D45	D75	D80	—	—
N_1（*kN*）	4.89*	4.42*	2.40	—	—
N_2（*kN*）	8.53	7.74	3.97	—	—
N_j（*kN*）	7.57	6.55	0*		
S	S1	S2	S3	—	—
N_1（*kN*）	3.23*	4.82*	5.96*	—	—
N_2（*kN*）	5.21	8.75	14.78	—	—
N_j（*kN*）	4.17	7.60	14.03		
R	R0	R100	R30	—	—
N_1（*kN*）	2.13	2.20	4.82	—	—
N_2（*kN*）	2.79	3.80	8.55	—	—
N_j（*kN*）	0*	0*	7.47		
A	A0	A10	A15	—	—
N_1（*kN*）	4.90*	4.39*	3.44*	—	—
N_2（*kN*）	8.57	7.45	5.27	—	—
N_j（*kN*）	7.63	6.80	4.80		

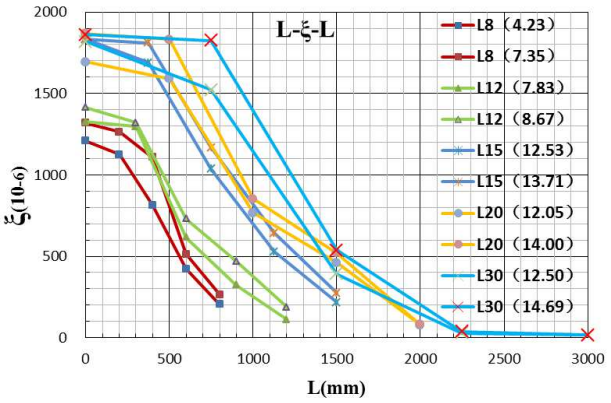

Fig 17 The curve of $L-\xi-L$.

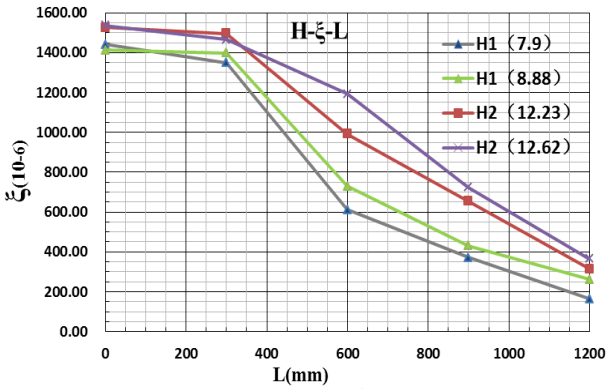

Fig 18 The curve of $H-\xi-L$.

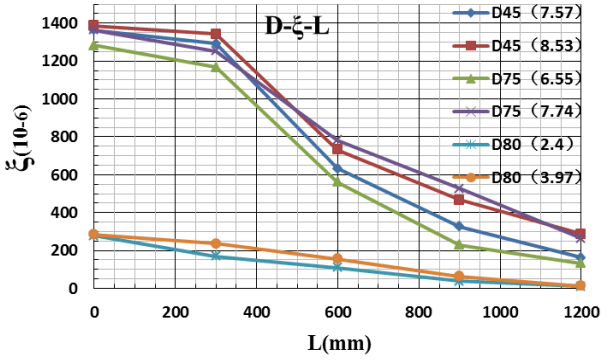

Fig 19 The curve of $D-\xi-L$.

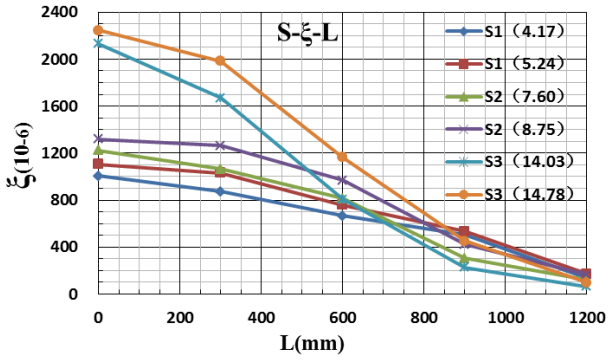

Fig 20 The curve of $S-\xi-L$.

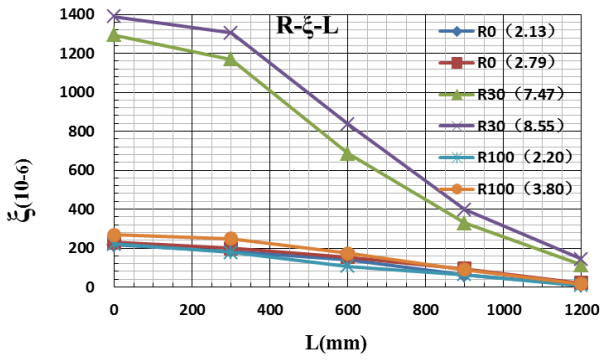

Fig21 The curve of $R-\xi-L$.

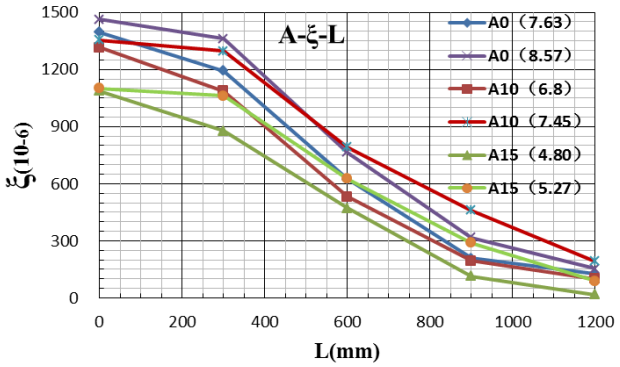

Fig22 The curve of $A-\xi-L$.

(1) Design value N of anchorage force based on the anchor length L.

According to the analysis from Figures 17-22, with the increase of anchorage length (L), grouting material strength S and geo-filament surface roughness R, the anchorage performance of geo-filament improves obviously; in which the anchorage length (L) has the most prominent impact on the performance of anchorage system, and the change of anchor length (L) is the most common in practical application.

According to Figure 17, the maximum transmission depth of the anchorage force of the geo-filament anchorage system is about 2.2 m, and the stress in the middle section of the anchor changes greatly. The longer the anchor length is, the more uniform the stress distribution is and the smaller the change of adjacent strain is. The stress distribution of anchor in 800 mm-1,200 mm section is significantly different from that in 1,500 mm-2,000 mm section. Based on the analysis of the anchor failure stage in Table 5, if the length of anchor is greater than 2 m, the grouting pull-out destruction mode occurs. In case of considering the possibility of subsequent failure of the reinforced earthen ruins, the destruction mode of filament pull-out is more conducive to the complete protection of the ruins on the premise of providing the required anchorage force. Therefore, the design value of the anchorage depth of geo-filament anchor should not be greater than 2 m, and the optimum length of anchorage is between 1.2 m and 1.5 m.

By comparing the strain distribution curve of anchor under the action of various combined anchorage force design values N, *the anchorage force design value* N *is determined based on the change of anchor length L, and the calculation formula is reasonable. Considering the safety stock of anchorage system and the anchorage performance, the calculation formula of* N *value is shown in Formula 3.*

$$N=\begin{cases} N_1 & 0<L<1500 \\ N_2 & 1500\le L\le 2000 \end{cases} \qquad (3)$$

(2) Grouting material strength design value.

In case of the destruction of the anchorage system between the slurry and the ruins, the anchorage performance can be brought into full play, which belongs to the ideal destruction position; however, this destruction mode causes damage to the ruins, which is not conducive to the protection of ruins soil cultural relics. Therefore, if the anchor is designed, it shall be considered that the failure section occurs between the slurry and the rod interface, and the ruins cannot be failed in case of failure in the later use process. The load of geo-filament anchor is mainly transmitted through the bond stress (shear stress) between the anchor and the slurry, and the failure form of the slurry is shear failure.

By comparing the stress distribution at the geo-filament-grouting interface in Figures 17-22 and comparing and analyzing the obtained data, it can be concluded that the L/5 section at the anchor end bears about 45% of the anchorage force under the action of anchorage force design value N,

and the damage of the anchorage system begins with the crack of the end grouting. After certain simplification, the stress distribution diagram of anchorage system of geo-filament anchor under the action of anchorage force N can be obtained, as shown in Figure 23.

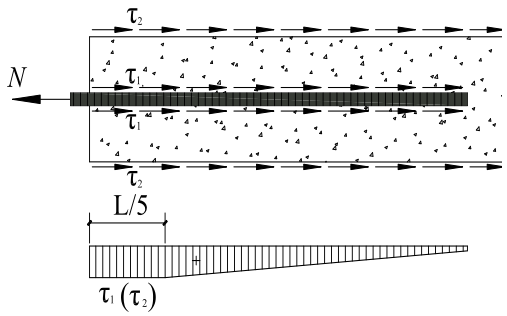

Fig23 Interface bond stress distribution diagram of GFA under N action.

In the Figure23, τ_1 represents the bond stress between the L/5 section of the geo-filament end and the grouting interface, and τ_2 represents the bond stress between the L/5 section grouting of the geo-filament end and the ruins soil interface. According to the balance of internal and external force, τ_1, τ_2 can be obtained as:

$$\tau_1 = \frac{9N}{8dL} \quad (4)$$

$$\tau_2 = \frac{9N}{4\pi DL} \quad (5)$$

Where d is the width of the geo-filament, and D depicts the bore diameter of grouting (Fig. 7). $\tau_1 = \frac{\pi D}{2d}\tau_2$ can be obtained from Equations (4) and (5), $\alpha = \frac{\pi D}{2d}$ is defined as the shear stress diffusion coefficient. The relationship of τ_1 and τ_2 can be written as:

$$\tau_2 = \frac{1}{\alpha}\tau_1 \quad (6)$$

Where we need to satisfy $\tau_2 \le \frac{\tau_2^{\max}}{n}$, and n is the safety factor. Therefore, the relation between τ_1 and τ_2 can be further written as:

$$\tau_1 \le \frac{\alpha}{n}\tau_2^{\max} \quad (7)$$

Through comprehensive analysis, it can be concluded that the shear strength of the grouting material should not be more than $\frac{\alpha}{n}$ times that of the soil for the design of the geo-filament bolt.

6. Conclusion and Reflection:

6.1 Test conclusions

In reinforcing small sliders for earthen architectural sites, a GFA has its advantages including easiness in installation, due to its relatively small perforation, and effectiveness in deformation control. A GFA employs a full-length bonding anchoring mechanism, of which an under-applied-force simulation reveal a failure process in three phases, namely filament deformation (elastic deformation), slurry cracking (plastic deformation) and Geo-filament dislodging (adhesive detachment). Its maximum anchoring force is primarily determined by the anchorage length (L). However, improvement of its force transmission mechanism and destruction mode could be achieved by adjusting its grouting material strength (S) and surface roughness (R).The design value of the anchorage force (N) is determined by the extreme value of pulling force in each phase of its destruction process and L. Approximate 45% of the N is supported by the segment, 1/5 of L, near the end of the bolt. The stress distribution at the soil-anchor interface could thus be simplified as a uniform distribution on the L/5 end segment and a triangular distribution on the rest. The shear strength of the slurry (S) should not exceed α times of the shear strength of the reinforced soil.

On the premise of providing the required anchorage force, the "flaky" rod can change the destruction mode of traditional anchor. Considering the possibility of failure in the life cycle of the reinforced earthen ruins, the anchorage system using "flaky" rod mostly fails in the form of filament pullout, which is more conducive to the complete protection of ruins, the anchorage depth of GFA should not be greater than 2 m, the optimal anchorage length should be between 1.2 m and 1.5 m, the number of filaments should not be greater than one filament, and the bore diameter should be between 40 mm and 50 mm.

6.2 Test defects

The test design scheme of this paper also has some defects, Since the salt in the concrete will subsequently promote the salt precipitation of the ruins, the addition of concrete to the grouting material does not conform to the concept of earthen ruins protection. In the comparative analysis of the test data, it was found that there are certain defects in the strain gauge arrangement in the length-affected test group. In the L12, L15, L20 and L30 test groups, test gauges shall be added, that is, strain gauges shall be placed at 800 mm in L12; strain gauges shall be placed at 800 mm and 1,200 mm in L15, and so on, to facilitate the comparison and analysis of data results.

Therefore, in the test and theoretical analysis of new reinforcement materials and reinforcement technologies, the characteristics of cultural relics shall be fully considered. We shall not rashly apply new materials or technologies to cultural relics protection projects by simply taking the quality of reinforcement materials and technical measures as the standard.

6.3 Technology reflection

The original purpose of this test is to test the anchorage performance of an anchorage technology used to reinforce small sliding mass in earthen ruins. With the development of the test, through the analysis of the test phenomenon and data, a new understanding of protection technology of earthen ruins has been produced.

The protection of earthen ruins has its own particularity, which is not that the stronger the reinforcement measures are, the better the effect is. The mechanical characteristics of cultural relics shall be considered to predict the possibility of damage in the life cycle of cultural relics. The anchorage calculation theory shall not copy the existing theories in the field of geotechnical engineering. It shall start from the characteristics of earthen ruins protection to form its own design concept and calculation method.

Availability of data and material statement:

The authors declared that all data generated or analysed during this study are included in this published article and its supplementary information files.

Competing interests statement:

The authors declared that they have no conflicts of interest to this work.

Funding:

This work was supported by the China Postdoctoral Science Foundation (2020M683672XB), the Youth Science and Technology Fund of XAUAT (ZR18040), Major Special Projects in the Thirteenth Five-Year Plan of China(2017YFC0702405)，Independent Research and Development project of State Key Laboratory of Green Building in Western China（LSZZ202017）.

Author contributions:

Wang Yulan contributed to the conception of the study, performed the experiment and wrote the manuscript;

Guo Jian performed the data analyses and wrote the manuscript;

Zhang Weixi performed the data analyses；

Lei Fan helped perform the analysis with constructive discussions.

Acknowledgements:

In the preparation of the paper, the authors hold gratitude for Mr. Xi Lin for his suggestions in proofreading and English wording. The authors would also like to express our special thanks to the reviewers for their constructive suggestions.

REFERENCES:

1. *SUN Man-li. Research status and development of the conservation of earthen sites. Science of Conservation and Archeology, 2007, 19(4): 64－69.*
2. *ZHANG Jing-ke, GUO Qing-lin, LI Zui-xiong, et al. Preliminary study on anchorage mechanism of earthen sites[M]. Lanzhou: Lanzhou University Press, 2014.*
3. *BENMOKRANE B, ZHANG B, CHENNOUF A. Tensive properties and pullout behaviour of AFRP and CFRP rods for grouted anchor applications. Construction and Building Materials, 2000, 14: 157－170.*
4. *RONG Yan, LI Yu-hu, CAO Jing, et al. Application of bakelite rod anchor in protection of Tang Hanguangmen entrance remains[J]. Journal of Shaanxi Normal University (Natural Science Edition), 2016, 44(3):69-74.*
5. *Zhang J K, Chen W W, Li Z X, Guo Z Q, Wang N. Analysis of in-situ anchoring characteristics of composite anchor containing steel bar (Φ22mm)[J]. Rock and Soil Mechanics, 2014, 35(11).3139—3147.*
6. *Xue Q F, Jin X B, Chen Y N, Yang X H, Jia X, Zhou Y K. The historical process of the masonry city walls construction in China during^{1st} to 17th centuries AD[J]. Plos One, 2019, 14(3): 1-16.*
7. *Li J F, Zhang J K, Wang Nan, Zhao L Y, Guo Q L. Physical model test on working mechanisms of an anchor group system with four wood bolts in rammed earthen sites[J]. Chinese Journal of Rock Mechanics and Engineering, 2019, 38(11): 2321—2331.*
8. *Cui K, Wang D H, Chen W W, Ren X F, Liu J, Yang G. Comparative study of anchorage performance of three types of bolts fully grouted by modified glutinous rice mortar[J]. Rock and Soil Mechanics, 2018, 39(2): 498—506.*
9. *LIU Guo-qing, XIAO Ming, CHEN Jun-tao, et al. Stress analysis method of fully grouted rock bolt in underground caverns[J]. Journal of Huazhong University of Science and Technology (Natural Science Edition), 2017, 45(6):113-119.*
10. *LU Wei, ZHAO Dong, LI Dong-bo, et al. Study on the force transfer process of the anchorage interface of bamboo bolt in the rammed earth sites[J]. Chinese Journal of Theoretical and Applied Mechanics, 2019, 51(2): 524-539.*
11. *ZHANG Jing-ke, CHEN Wen-wu, LI Zui-xiong, et al.Field tests on anchorage mechanism of wood bolts for conservation of earthen sites. Chinese Journal of Geotechnical Engineering, 2013, 35(6): 1166－1171.*
12. *Lu W, Zhao D, Mao XF, et al. Experimental study on bond-slip behavior of bamboo bolt-modified slurry interface under pull-out load.Advances in Civil Engineering, 2018.01: 1-23.*
13. *Wang Yulan, Dong Zhao, Wei Lu , and Lei Fan. Experimental Research on Destruction Mode and Anchoring Performance of Carbon Fiber Phyllostachys pubescens Anchor Rod with Different Forms. Advances in Civil Engineering, 2018.03: 1-13.*
14. *Zhang J K, Shan T T, Wang Y C, Wang N, Meng F, Zhao L Y. Mechanical properties of the soil-slurry (CGN+C) interface of anchorage system in earthen sites[J]. Rock and Soil Mechanics, 2019, 40(3): 903-912.*
15. *Peng Wenxiang，Xie Yujun，Xu Songshan，et al． Test study on working properties of prestress anchor composite soil nails wall work．Journal of Southeast University,2015,46(4):1468-1474．*
16. *H. C. Biscaia, C. Chastre, and M. A. G. Silva, "Linear and nonlinear analysis of bond-slip models for interfaces between FRP composites and concrete," Composites Part B: Engineering, vol. 45, no. 1, pp. 1554–1568, 2013.*
17. *Chen Y. Experimental study and stress analysis of rock bolt anchorage performance. J Rock Mech Geotech Eng. 2014, 6:428–437*
18. *L. B. Martin, M. Tijani, and F. Hadj-Hassen, "A new analytical solution to the mechanical behavior of fully grouted rock bolts subjected to pull-out tests," Construction and Building Materials, vol. 25, no. 2, pp. 749-255, 2011.*
19. *RENFF, YANGZJ, CHENJF, et al. An analytical analysis of the full-range behaviour of grouted rockbolts based on a tri-linear bond-slip model. Construction and Building Materials, 2010, 24: 361－370*
20. *Nie W, Zhao Z Y, Guo W, Shang J, Wu C. Bond-slip modeling of a CMC rock bolt element using 2D-DDA method[J]. Tunnelling and Underground Space Technology, 2019, 85, 340—353.*

21. *Wang Z W, Zhao J C, Liu T B. Bond-slip model for horizontal reinforcing bars in reinforced brick masonry[J]. Engineering Structure, 2019, 201: 109770.*
22. *WU Zhi-min, YANG Shu-tong, ZHENG Jian-jun, et al. Analytical solution for the pull-out response of FRP rods embedded in steel tubers filled with cement grout. Material and Structures, 2010, 43: 597—609*
23. *LU Wei, ZHAO Dong, LI Dong-bo, et al. Study on the force transfer process of the anchorage interface of bamboo bolt in the rammed earth sites[J]. Chinese Journal of Theoretical and Applied Mechanics, 2019, 51(2): 524-539.*
24. *CUI Kai, HUANG Jing-jing, CHEN Wen-wu, et al. Researches on selection of anchor slurry and performance mixed quick lime in earthen ruins[J]. Rock and Soil Mechanics, 2019, 40(6): 2183-2191.*

Supplementary Files

This is a list of supplementary files associated with this preprint. Click to download.

- data.xlsx